The 2025 World Congress on
Advances in Structural Engineering and Mechanics (ASEM25)
BEXCO, Busan, Korea, August 11-14, 2025

Development of Physically-Based Model for Shallow Landslides in Natural Terrain

Joon-Young Park[1)], Young-Suk Song[2)], Minsun Lee[3)], and *Seongwon Hong[4)]

[1), 2)] *Geological Hazard Research Department, Geological Safety Division, KIGAM, Daejeon 34132, Korea*
[3)] *Hydro Technology Institute Co.,Ltd., Nakanoshima Kita-ku Osaka 530-6126, Japan*
[4)] *Department of Safety Engineering, Korea National University of Transportation, Chungju, Korea*
[4)] shong@ut.ac.kr

ABSTRACT

This study integrates surface runoff analysis, subsurface infiltration analysis, and infinite slope stability analysis that incorporates matric suction of unsaturated soils to examine rainfall-induced shallow landslides occurring on natural slopes. By combining these analytical methods, we aimed to develop a physically-based predictive model capable of evaluating shallow landslide susceptibility triggered by rainfall events.

1. INTRODUCTION

Most landslides occur predominantly during rainy seasons, suggesting rainfall as the primary triggering factor. In Korea, the majority of annual rainfall is concentrated between June and September, leading to frequent landslides caused by heavy rainfall, with damage increasing significantly each year (Kim and Song 2015). Examining landslide occurrences in Korea, most are shallow planar failures, typically within a depth of 2 meters (Kim and Song 2015). Rainfall-induced landslides are commonly attributed to increased pore water pressure within slopes due to rising groundwater levels. However, in natural slopes, shallow landslides predominantly result from the downward migration of the wetting front caused by rainfall infiltration rather than from groundwater level rise (Kim et al. 2004; Lu and Godt 2008; Song et al. 2012). Rainfall infiltration increases saturation in unsaturated soils above the groundwater table, thereby reducing negative pore water pressures. This change in suction stress consequently decreases effective

---

[1)] Senior Researcher
[2)] Principal Researcher
[3)] Project Manager
[4)] Associate Professor

stress, significantly affecting the stability of unsaturated slopes (Ng and Shi 1998; Lu and Godt 2008). Therefore, considering variations in effective stress at different soil depths above the groundwater table is critical, as slope failures occur due to moisture content changes within this unsaturated soil layer during rainfall events. To analyze shallow failures occurring during rainfall in natural slopes in Korea, it is essential to develop physically-based landslide prediction models. Rainfall infiltrates the subsurface and generates surface runoff, requiring an integrated analysis of both surface water and groundwater flow. Moreover, during rainfall infiltration, soil layers transition from unsaturated to saturated conditions, necessitating two-phase flow analysis (water-air) within the unsaturated zone. Based on this, an infinite slope stability analysis incorporating suction stress within unsaturated soils should be applied to evaluate the factor of safety against shallow slope failure during rainfall.

Consequently, this study applies surface runoff analysis, subsurface infiltration analysis, and infinite slope stability analysis considering suction stress in unsaturated soils to analyze shallow slope failures in natural slopes during rainfall. Integrating these analyses, we aim to develop a physically-based landslide prediction model capable of analyzing shallow rainfall-induced landslides.

2. MODEL DEVELOPMENT

To develop a new physically-based prediction model for shallow landslides induced by rainfall in natural slopes in Korea, we conducted surface runoff analysis, subsurface water flow analysis, and infinite slope stability analysis considering suction stress in unsaturated soils.

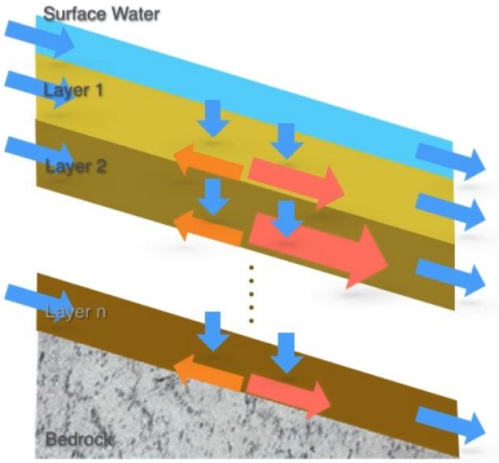

Fig. 1 Conceptual Diagram of Shallow Landslides Induced by Rainfall

Fig. 1 illustrates a conceptual schematic for evaluating surface runoff, rainfall infiltration, and infinite slope stability during rainfall events. As shown, intense rainfall causes simultaneous surface runoff and subsurface infiltration. Hence, an integrated analysis of surface water and groundwater flow, two-phase flow analysis of water-air within unsaturated soil layers, and infinite slope stability analysis incorporating suction

stress were applied. Consequently, the physically-based landslide prediction model suitable for Korean natural slopes developed in this study integrates three analytical methods, namely surface water flow analysis, subsurface infiltration analysis, and infinite slope stability analysis considering suction stress, as depicted in Fig. 2.

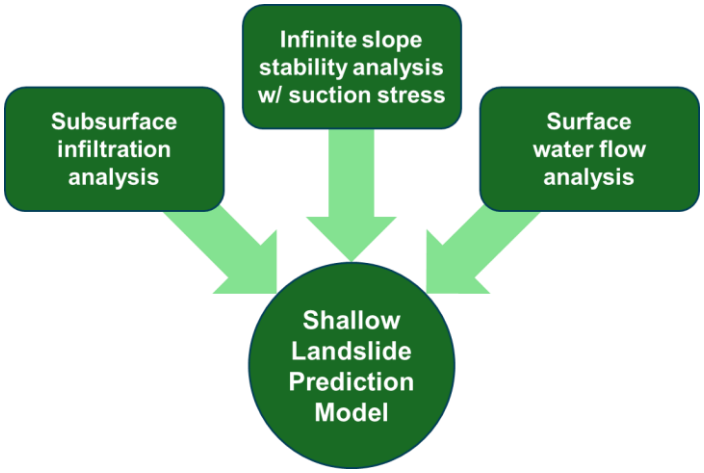

Fig. 2 Physically-based Landslide Prediction Model Suitable for Natural Slopes in Korea

2.1 Subsurface Infiltration Analysis

In shallow soil layers, groundwater flow occurs as two-phase water-air flow, expressed by the continuity equation as:

$$\frac{\partial\left(\rho_p \phi S_p\right)}{\partial t} = -\nabla \bullet F_p - \rho_p q_p \qquad (p = w, g), \tag{1}$$

where ρ_p is density [kg/m³], ϕ is porosity, S_p is saturation, t is time, F_p is flow rate [kg/m²/s], $\rho_p q_p$ is the flow rate increment per unit volume in the soil layer [kg/m³/s], and the subscript p, w, and g denote the soil layer, water, and air, respectively. The flow rate is calculated as:

$$F_p = \rho_p u_p = -\frac{\rho_p k_{rp} k}{\mu_p} \nabla\left(P_p + \rho_p g z\right), \tag{2}$$

Here, u_p represents Darcy velocity [m/s], k absolute permeability [m²], k_{rp} relative permeability, μ_p viscosity [Pa·s], P_p pressure of the soil layer [Pa], and g gravitational acceleration [m/s²].

Substituting Eq. (2) into Eq. (1) yields:

$$\frac{\partial\left(\rho_p \phi S_p\right)}{\partial t} = \nabla \left\{\frac{\rho_p k_{rp} k}{\mu_p} \nabla\left(P_p + \rho_p g z\right)\right\} - \rho_p q_p, \tag{3}$$

The potential Φ_p in the soil layer is defined by:

$$\Phi_p = P_p + \rho_p g z \,, \tag{4}$$

Substituting Eq. (4) into Eq. (3) gives:

$$\frac{\partial\left(\rho_p \phi S_p\right)}{\partial t} = \nabla \cdot \left\{ \frac{\rho_p k_{rp} k}{\mu_p} \nabla \Phi_p \right\} - \rho_p q_p \,, \tag{5}$$

The pressures of water P_w and air P_g in the soil layer relate as:

$$P_g - P_w = P_c \,, \tag{6}$$

Here, P_c is the capillary pressure [Pa], and the saturation of water and air in the soil layer is related by the following equation:

$$S_w + S_g = 1 \,, \tag{7}$$

Capillary pressure and relative permeabilities follow van Genuchten (1980) and Corey (1954) models, respectively, as shown in Eqs. (8) to (10).

$$S_{we} = \left\{ 1 + \left(\alpha |h| \right)^n \right\}^{-m} \,, \tag{8}$$

$$k_{rw} = \sqrt{S_{we}} \left\{ 1 - \left(1 - S_{we}^{\frac{1}{m}} \right)^m \right\}^2 \,, \tag{9}$$

$$k_{rg} = \left(1 - S_{we}^2 \right) \left(1 - S_{we} \right)^2 \,, \tag{10}$$

Here, h is suction [m], and α, n, m are parameters of the van Genuchten model with the relation $m = 1 - 1/n$. The effective saturation in the soil layer S_{we} can be expressed as:

$$S_{we} = \frac{S_w - S_{wr} - S_{gr}}{1 - S_{wr} - S_{gr}} \,, \tag{11}$$

where S_{wr} is the residual water saturation in the soil, and S_{gr} is the residual air saturation. Water is assumed to be incompressible and represented as a function of pressure. Air is treated as an ideal gas.

$$\rho_w = \rho_{w,0} \left\{ 1 + c_w \left(P - P_0 \right) \right\} \,, \tag{12}$$

$$\rho_g = \rho_{g,0} \frac{P}{P_0}, \tag{13}$$

The densities of water and air, $\rho_{w,0}$ and $\rho_{g,0}$, are referenced at atmospheric pressure conditions at 20°C. Specifically, $\rho_{w,0} = 998.23\ [kg/m^3]$ and $\rho_{g,0} = 1.205\ [kg/m^3]$ at $P_0 = 0.101325\ [\mathrm{MPa}]$. The compressibility of water c_w is $0.45 \times 10^{-9}\ [1/\mathrm{Pa}]$, and the viscosity of water μ_w is assumed to vary linearly with pressure:

$$\mu_w = \mu_{w,0} \left\{ 1 + c_\mu \left(P - P_0 \right) \right\}, \tag{14}$$

Here, $\mu_{w,0}$ is the viscosity of water at atmospheric pressure, $1.002 \times 10^{-3}\ [\mathrm{Pa \cdot s}]$, and c_μ represents the rate of viscosity increase, $1 \times 10^{-9}\ [1/\mathrm{Pa}]$. Air viscosity μ_g is considered constant at $18.2 \times 10^{-6}\ [\mathrm{Pa \cdot s}]$ due to the relatively low-pressure variations.

2.2 Surface Water Flow Analysis

Assuming shallow-water flow, the two-dimensional surface flow continuity equation is:

$$\frac{\partial h_s}{\partial t} = -\nabla \cdot \left(h_s v \right) - q, \tag{15}$$

where h_s is depth [m], v average flow velocity [m/s], and q inflow from groundwater infiltration or rainfall [m/s]. Using the diffusive approximation, the motion equation for flow in a one-dimensional channel with a slope i_g is:

$$i_g + \frac{\partial h_s}{\partial x} \cos^2 \beta + \frac{n^2 v^2}{R^{4/3}} = 0, \tag{16}$$

Here, i_g is channel slope ($= \partial z / \partial x$), n Manning's roughness coefficient [$m^{-1/3}s$], and R average depth [m]. Eq. (16), solved for depth , yields Eq. (17):

$$v = -\frac{R^{2/3}}{n} \sqrt{\left| i_g + \frac{\partial h_s}{\partial x} \cos^2 \beta \right|} \operatorname{sgn}\left(i_g + \frac{\partial h_s}{\partial x} \cos^2 \beta \right), \tag{17}$$

$$\left| i_g + \frac{\partial h_s}{\partial x} \cos^2 \beta \right|^{1/2} \approx \left| i_g \right|^{1/2}, \tag{18}$$

Substituting Eq. (18) into Eq. (17), we obtain:

$$v = -\frac{R^{2/3}}{n\left|i_g\right|^{1/2}}\left(i_g + \frac{\partial h_s}{\partial x}\cos^2\beta\right), \tag{19}$$

This formulation is known as the linearized diffusion approximation model, representing an intermediate state between the kinematic wave model and the diffusion approximation model. This approximation is generally valid for natural water flows, demonstrating excellent stability and solutions closely aligning with diffusion solutions.

2.3 Infinite Slope Stability Analysis Considering Suction Stress

The analysis assumes an infinite slope with uniform soil depth and homogeneous soil, inclined at an angle β. Fig. 3 shows a segment of the infinite slope for deriving stability equations.

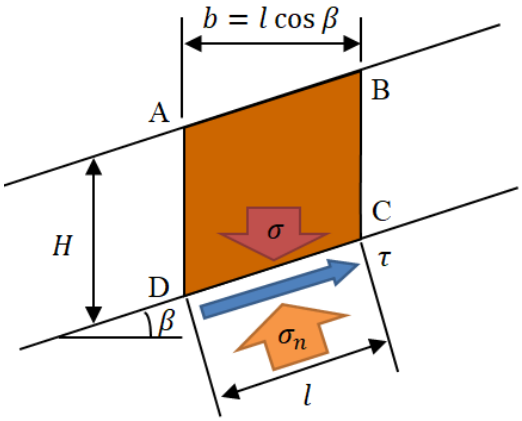

Fig. 3 Physically-based Landslide Prediction Model Suitable for Natural Slopes in Korea

Considering a parallelogram-shaped soil element ABCD with unit width, its weight (W) is calculated as:

$$W = \gamma_t Hb \cdot 1 = \gamma_t Hl\cos\beta, \tag{20}$$

where γ_t is the moist unit weight [N/m³]. The shear force S acting along the slope on the soil element is determined by:

$$S = W\sin\beta = \gamma_t Hl\sin\beta\cos\beta, \tag{21}$$

The vertical stress on the base area ($l \times 1$) of the soil element is expressed by:

$$\sigma = \frac{W}{l\times 1}\gamma_t H\cos\beta, \tag{22}$$

Thus, the vertical stress component (σ_n) acting on the base of the soil element is calculated by:

$$\sigma_n = \sigma \cos\beta = \gamma_t H \cos^2\beta \,, \tag{23}$$

According to Coulomb's failure criterion, the shear strength acting on the failure plane can be expressed as:

$$\tau = c + \sigma_n' \tan\phi \,, \tag{24}$$

Here, c is cohesion [N/m²], σ_n' is effective stress [N/m²], and ϕ is the internal friction angle. The effective stress is calculated using an equation proposed by Lu and Likos (2004, 2006) that considers both saturated and unsaturated states:

$$\sigma_n' = \sigma_n - \sigma^s \,, \tag{25}$$

where σ^s is suction stress [N/m²]. Suction stress can be determined based on soil saturation:

$$\sigma^s = -\left(P_a - P_w\right) \qquad P_a - P_w \le 0 \,, \tag{26}$$

$$\sigma^s = -\frac{\theta - \theta_r}{\theta_s - \theta_r}\left(P_a - P_w\right) = -S_{we}\left(P_a - P_w\right) \qquad P_a - P_w > 0 \,, \tag{27}$$

Here, P_a is pore air pressure [N/m²], P_w is pore water pressure [N/m²], θ is volumetric water content, θ_s is saturated volumetric water content, θ_r is residual volumetric water content, and S_{we} is effective saturation. For saturated soil, effective stress is obtained by substituting Eq. (26) into Eq. (25):

$$\sigma_n' = \sigma_n - \left(P_w - P_a\right) \,, \tag{28}$$

This indicates that effective stress is smaller than the vertical stress by the pore water pressure. Conversely, for unsaturated soils, suction stress (σ^s) from Eq. (27) is negative, resulting in effective stress exceeding vertical stress. Suction stress encompasses localized forces such as van der Waals forces at particle contacts, electrostatic forces from electrical double layers, and surface tension, integrated as macroscopic stresses. Assuming uniform shear strength on the CD plane in Fig. 3, shear resistance (R) is calculated using Eqs. (23) and (24):

$$R = \tau l \;\square 1 = l[c + \sigma_n' \tan\phi] = l[c + \left(\gamma_t H \cos^2\beta - \sigma^s\right)\tan\phi] \,, \tag{29}$$

Thus, the factor of safety (F_s) is determined by the ratio of Eqs. (21) and (29):

$$F_s = \frac{R}{S} = \frac{c + \left(\gamma_t H \cos^2\beta - \sigma^s\right)\tan\phi}{\gamma_t H \sin\beta\cos\beta} = \frac{\tan\phi}{\tan\beta} + \frac{2c}{\gamma_t H \sin 2\beta} - \frac{\sigma^s}{\gamma_t H}\left(\tan\beta + \cot\beta\right)\tan\phi \quad , \tag{30}$$

In Eq. (30), the terms represent internal friction angle, cohesion, and suction stress, respectively.

3. CASE STUDY FOR MODEL VALIDATION

To validate the accuracy of the physically-based landslide prediction model, comparative analyses were conducted based on historical landslide data from Mt. Jiri. As depicted in Fig. 4(a), accumulated rainfall exceeding approximately 350 mm occurred from July 31 to August 8, 2014, around the Mt. Jiri area, resulting in numerous landslides. In the figure, the blue circles indicate landslide initiation points, while the other blue areas represent runout zones. Fig. 4(b) presents the results analyzed by the physically-based model for the corresponding landslide event. It can be observed that the actual landslide occurrence areas closely match the model-predicted areas, with very minimal false positive regions.

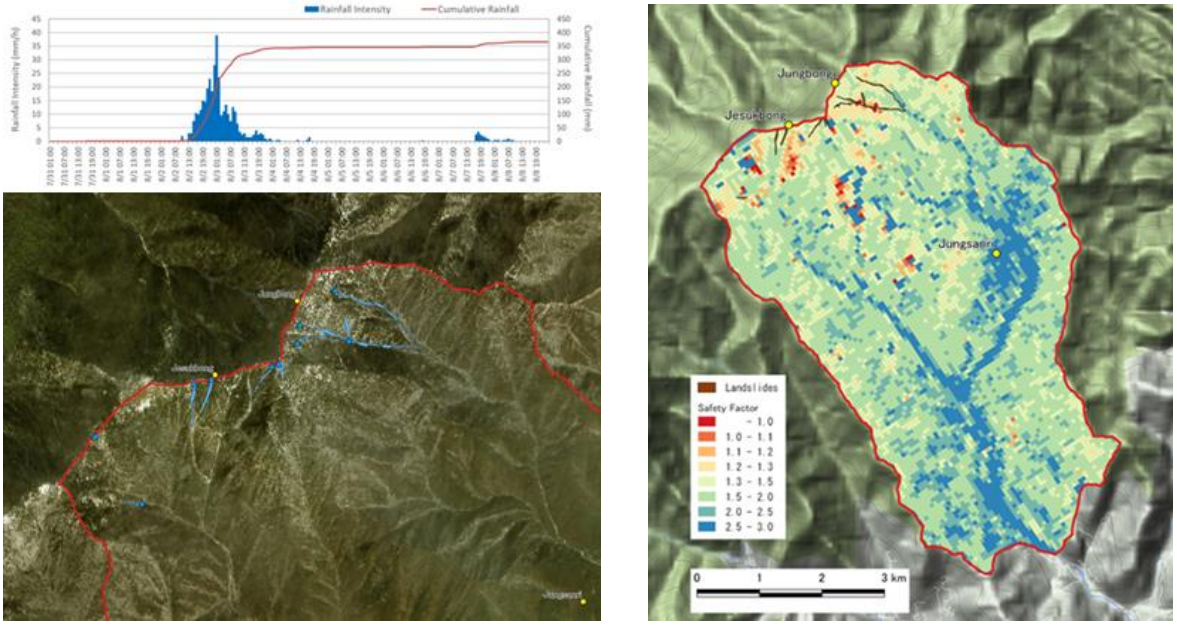

(a) (b)

Fig. 4 2014 Mt. Jiri landslides: (a) occurrence status and rainfall records, (b) physically-based prediction results

Since late 2014, four landslide monitoring stations have been established and operated in the southeastern area of Mt. Jiri (covering 20.6 km²). These stations conducted field investigations of soil depth and comprehensive soil characterization

analyses, including engineering and unsaturated soil properties (Fig. 5). Fig. 6 illustrates a schematic of installed monitoring equipment, including tensiometers, TDR sensors, tiltmeters, rain gauges, and master loggers.

Fig. 5 Establishment of landslide monitoring stations in the southeastern region of Mt. Jiri

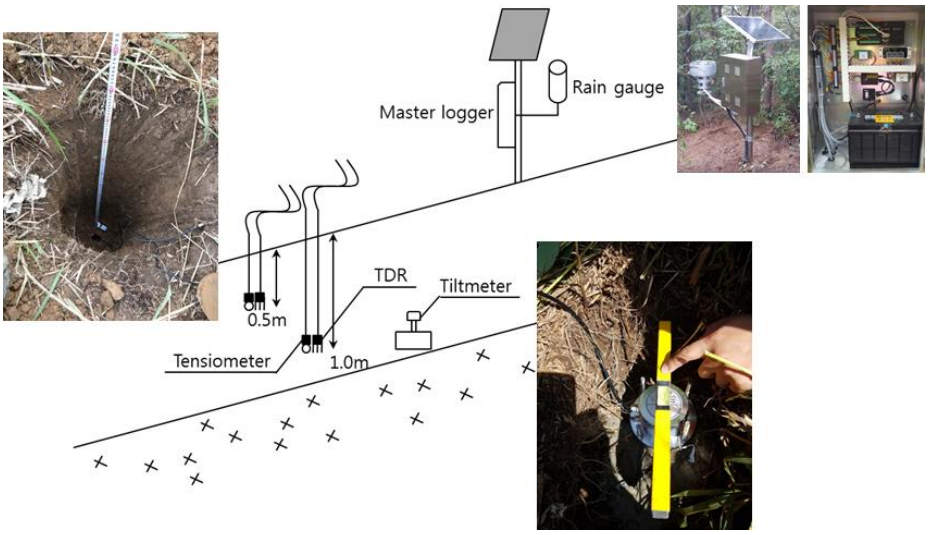

Fig. 6 Sensor components installed at the landslide monitoring stations

To verify the accuracy of the developed physically-based landslide prediction model, volumetric water content (VWC) data monitored from 2015 to 2016 were compared against VWC values calculated by the model during the summer seasons. Figs. 7 and 8 present comparisons between the monitored and calculated VWC data for the corresponding periods. As observed, the variations in VWC induced by rainfall events were highly consistent between the measured (or observed) data from the monitoring stations and the predictions (or calculated data) from the physically-based model.

Therefore, the landslide prediction model developed through this research demonstrates high accuracy and practical field applicability.

Fig. 7 Comparison of Field Monitoring Results and Physically-Based Model Predictions in 2015. * Obs.: Observed Data, Calc.: Calculated Data, Upper: Upper Slope, Lower: Lower Slope, GL: Ground Level

Fig. 8 Comparison of Field Monitoring Results and Physically-Based Model Predictions in 2016. * Obs.: Observed Data, Calc.: Calculated Data, Upper: Upper Slope, Lower: Lower Slope, GL: Ground Level

4. CONCLUSIONS

Recent landslide models utilize static topographic indices or dynamic hydrologic indices (e.g., Montgomery and Dietrich 1994; Tarolli and Tarboton 2006) for efficient interpretation of landslide mechanisms, prompting ongoing research into downslope flow

processes originating from ridge tops within the framework of hillslope hydrology. This study developed and validated a comprehensive physically-based model integrating surface runoff analysis, subsurface infiltration analysis, and infinite slope stability analysis that incorporates suction stress in unsaturated soils to predict rainfall-induced shallow landslides in natural terrains.

The developed physically-based model demonstrated high predictive accuracy when validated against historical landslide events in the Mt. Jiri region. Comparative analyses using calculated and monitored volumetric water content (VWC) showed close agreement between model predictions and field observations, with minimal false-positive occurrences. This validation underscores the robustness and practical applicability of the model for real-world landslide hazard assessments.

The originality of this research lies in its integrated approach, combining surface and subsurface hydrological processes with unsaturated soil mechanics to accurately model landslide initiation mechanisms. This comprehensive methodology enables precise identification and assessment of landslide-prone areas, significantly contributing to improved landslide early warning systems and risk mitigation strategies.

The expected outcomes from applying this physically-based model include enhanced accuracy in landslide susceptibility mapping, improved preparedness through timely early warnings, and better-informed decision-making for disaster management authorities. Future research should focus on refining input parameters to reduce uncertainties, particularly concerning spatial variability in soil properties and hydrological characteristics. Additionally, extending the model application to various geological and climatic conditions could further validate its versatility and effectiveness, paving the way for broader implementation in landslide-prone regions globally.

REFERENCES

Corey, A. T. (1954), “The interrelation between gas and oil relative permeabilities”, *Producers Monthly*, **19**, 38-41.

Kim, J.H., Jeong, S.S., Park, S.W. and Sharma, J. (2004), “Influence of rainfall-induced wetting on the stability of slopes in weathered soils”, *Engineering Geology*, **75**, 251-262.

Kim, K.S. and Song, Y.S. (2015), “Geometrical and geotechnical characteristics of landslides in Korea for various geological conditions”, *Journal of Mountain Science*, **12(5)**, 1267-1280.

Lu, N. and Godt., J. (2008), “Infinite-Slope Stability under Steady Unsaturated Seepage Conditions”, *Water Resources Research*, **W11404**, **44**, 1-13.

Lu, N. and Likos, W.J. (2004), “Unsaturated soil mechanics,” *John Wiley & Sons Inc.*, New York, 556.

Lu, N. and Likos, W.J. (2006), “Suction stress characteristic curve for unsaturated soil”, *Journal of Geotechnical and Geoenvironmental Engineering*, *ASCE*, **132(2)**, 131-142.

Montgomery, D.R. and Dietrich, W.E. (1994), “A physically based model for the topographic control on shallow landsliding”, *Water Resources Research*, **30(4)**, 1153-1171.

Ng, C.W.W. and Shi, Q. (1998), “A numerical investigation of the stability of unsaturated soil slopes subjected to transient seepage”, *Computers and Geotechnics*, 22(1), 1-28.

Song, Y.S., Hong, W.P. and Woo, K.S. (2012), "Behavior and analysis of stabilizing piles installed in a cut slope during heavy rainfall", *Engineering Geology*, **129-130**, 56-67.

Tarolli, P. and Tarboton, D.G. (2006), "A new method for determination of most likely landslide initiation points and the evaluation of digital terrain model scale in terrain stability mapping", *Hydrology and Earth System Sciences*, **10(5)**, 663-677.

van Genuchten, M.T. (1980), "A closed-form equation for predicting the hydraulic conductivity of unsaturated soils", *Soil Science Society of America Journal*, **44**, 892-898